DOE/ET-53088-261 IFSR #261

Effective Diffusion in Laminar Convective Flows

M. N. Rosenbluth, H. L. Berk, I. Doxas
and *W. Horton*

Institute for Fusion Studies
The University of Texas at Austin
Austin, Texas 78712

March 1987

Effective Diffusion in Laminar Convective Flows

M. N. Rosenbluth, H. L. Berk, I. Doxas,

and *W. Horton*

Institute for Fusion Studies

The University of Texas at Austin

Austin, Texas 78712

Abstract

The effective diffusion coefficient D^* of a passive component, such as test particles, dye, temperature, magnetic flux, etc., is derived for motion in periodic two-dimensional incompressible convective flow with characteristic velocity v and size d in the presence of an intrinsic local diffusivity D. Asymptotic solutions for effective diffusivity $D^*(P)$ in the large P limit, with $P \sim vd/D$, is shown to be of the form $D^* = cDP^{1/2}$ with c being a coefficient that is determined analytically. The constant c depends on the geometry of the convective cell and on an average of the flow speed along the separatrix. The asymptotic method of evaluation applies to both free boundary and rough boundary flow patterns and it is shown that the method can be extended to more complicated patterns such as the flows generated by rotating cylinders, as in the problem considered by Nadim, Cox, and Brenner [J. Fluid Mech. **164**, 185 (1986)]. The diffusivity D^* is readily calculated for small P, but the evaluation for arbitrary P requires numerical methods. Monte Carlo particle simulation codes are used to evaluate D^* at arbitrary P, and thereby describe the transition for D^* between the large and small P limits.

I. INTRODUCTION

In this work we calculate the effective diffusion of a passive component (such as test particles, dye, temperature, etc.) in a laminar flow pattern when there is a local diffusion present, with a diffusivity D, due to collisions or fluctuations. This problem is of interest in both fluids and plasmas where two-dimensional laminar flow patterns are encountered as the stationary states of driven systems. Classical examples are the two-dimensional rolls of the Rayleigh-Benard problem and the Taylor vortices in Couette flow[1] and heat flow in a convecting fluid.[2–6] Analogous problems arise in magnetized plasmas in such examples as the saturated state of the drift wave instability driven by the ion temperature gradient,[7] various weakly unstable magnetohydrodynamic instabilities,[8] and the generation of magnetic field from the passive convection of magnetic flux.[9,10] The effective diffusion of dye immersed in a laminar convecting fluid has also been of some recent experimental interest,[11–13] although turbulence and fluctuations, which will not be treated here, appear to be playing an important role in the experimental phenomena.

In these problems each passively convected component has its own characteristic diffusivity D in the rest frame of the material. It is well known that the actual transport of the passive component driven by a large-scale spatial gradient gives rise to an enhanced effective diffusivity D^* due to the increased transport from the convective motion. For a convective cell with a flow velocity v and characteristic size d, the enhancement is a function of the Peclet number $P = vd/D$. For small P the enhancement varies as $D^* = D\left(1 + aP^2\right)$ with constant a.[3,4] For large Peclet number, boundary layers form along the separatrix of the convective cells where sharp gradients of the passive component occur. In this regime, matched asymptotic methods are used to calculate the flux across the separatrix. The analysis shows that enhanced diffusion varies as $D^* = cDP^{1/2}$ with constant c.

Rather surprisingly, the detailed calculation of the enhanced diffusion for typical simple periodic flow patterns has not been addressed until recently. The general result of a $P^{1/2}$ enhancement has been noted by Moffat,[9] while the analysis of Sagues and Horsthemke[14] for the enhancement only applies to the small Peclet number regime. Nadim et al.[15] treat the diffusion of a more complicated flow due to a periodic set of rotating cylinders. This flow is topologically similar to the flow treated in the present work and we show in the

appendix how our analysis can be generalized to describe the problem solved numerically in Ref. 15. During the course of this work we have found that Shraiman[16] and Perkins and Zweibel[10] have also calculated D^* in the limit of large P by generalizing methods described in Refs. 5 and 6. These methods require numerical solution of an integral equation, which are often subject to numerical inaccuracy.

In this work we calculate in detail the effective diffusivity D^* for the two-dimensional incompressible flow velocity given by $\vec{u} = \hat{\mathbf{z}} \times \nabla\psi(x,y)$ where the stream function $\psi(x,y)$ is given in the first part of the paper by

$$\psi = \psi_0 \sin\left(\frac{\pi x}{d}\right) \sin\left(\frac{\pi\beta y}{d}\right).$$

The calculation for small P is a straightforward second order perturbation calculation.[2,3,13] A new technique, particularly well suited for periodic flows, is developed for calculating D^* for large P from which a complete analytic solution is obtained. Our method differs from the matched asymptotic method previously employed[2,7,12,14] and does not require numerical solution of an integral equation.

We show that $D^* = cDP^{1/2}$, with the dependence of c on the geometry of the convective cell given. We also generalize our calculation to more general periodic convection geometries. Specifically, we show that the method can be applied to the flow past a rough rigid wall and for even more complicated flows like those treated Nadim et al.[15] The result $D^* = cDP^{1/2}$ remains the dominant form of the enhancement as noted in Ref. 15.

The solution for arbitrary P still remains difficult to obtain analytically. To study the complete range of P we have developed a Monte Carlo code that uses two different methods to measure the transport produced by the diffusion D in the given convective flow. In the steady-state method, the flux of particles out of a unit cell is calculated in the steady state by introducing boundary sources determined by and justified from the formal method developed here in deriving the steady-state flux. In the initial value method, the running diffusion coefficient of a freely evolving initial distribution is measured along with the particle (Lagrangian) correlation time.

The structure of this paper is as follows. In Sec. II we develop our formalism for the special choices of the stream functions and solve for the effective diffusivity in the small

and large Peclet number limits. In Sec. III we extend the method to treat general stream functions including flows along rough walls. In Sec. IV we present the method and results of the Monte Carlo calculation. In Sec. V we summarize the results of this work. In the appendix we generalize our method of calculation to solve analytically the rotating cylinder problem described in Ref. 15.

II. BOUNDARY LAYER CALCULATION FOR FLUX ACROSS CELL BOUNDARIES

In this section we calculate the effective diffusion in a simple laminar periodic flow pattern. Such a situation might arise, for example, if we were to study the spreading of dye in a Benard convection pattern. We are concerned with the case of simple laminar two-dimensional incompressible flow. The governing equation for the density of the dye is

$$\frac{\partial n}{\partial t} + \mathbf{u} \cdot \nabla n = D\nabla^2 n, \tag{1}$$

where D is the molecular diffusion coefficient and u the given fluid velocity which for a single mode is of the form

$$\mathbf{u} = \frac{\tilde{u}d}{\pi}\hat{\mathbf{z}} \times \nabla\psi \tag{2}$$

with the streamline function

$$\psi = \sin\pi\frac{x}{d}\sin\pi\beta\frac{y}{d}. \tag{3}$$

Thus d gives the size of a roll, β its aspect ratio, and $\tilde{u}$ the maximum flow velocity in the y-direction. Figure 1 shows a segment of the flow pattern. The boundary of a roll is given by $\psi = 0$, the center by $\psi = 1$.

We want to calculate the effective diffusion coefficient for spreading of a dye in the limit that the overall scale length of the density gradient is much larger than d and the times of interest are much longer than the characteristic roll times we discuss below. Thus, if we look over distances large compared to a roll size, but small compared to the overall spread of the dye, the density near a point (x_i, y_i) is given by

$$n = n_0(x_i, y_i) + (x - x_i)\frac{\overline{\partial n_0}}{\partial x} + (y - y_i)\frac{\overline{\partial n_0}}{\partial y} + n_p(x, y), \tag{4}$$

where $\overline{\partial n_0/\partial x}$ and $\overline{\partial n_0/\partial y}$ are the components of the global density gradient at (x_i, y_i). Here, n_p is a periodic fine structure to the density on the scale of the rolls. The effective diffusion we wish to calculate will lead to slow changes in time of n_0 as is characteristic of a diffusive process. Since this is a linear problem for n, the solution will be a superposition of identical linear forms (to within a scaling factor) proportional to $\overline{\partial n_0/\partial x}$ and $\overline{\partial n_0/\partial y}$. Thus, we lose no generality by specifying the global gradient to be in the x-direction and choosing $(x_i, y_i) = 0$. Subsequently, we denote $\overline{\partial n_0/\partial x} = \bar{n}_0'$.

The microstructure introduced by the flow is characterized by two characteristic times: $\tau_H = d/\tilde{u}\beta$ the time for circulation around the roll, and $\tau_D = d^2/D$ the time for molecular diffusion of a particle through a roll. The ratio τ_D/τ_H is known as the Peclet number P. Since molecular diffusion is generally a very slow process, the physical situation of interest is that of $P \gg 1$ with which we are primarily concerned. We may note in passing that in the opposite limit $P \ll 1$ the effective diffusion coefficient D^* simply equals the molecular diffusion coefficient D, with small corrections that have been calculated by several authors.

Before passing to a detailed mathematical description of the problem for $P_e \gg 1$, we elucidate the governing physics in terms of a random walk. Consider the dye particles within a given roll, and how they will move during a time τ_H. Those confined in the interior of a roll will simply circulate around it. However, those close to the edge in a boundary layer may diffuse across a roll boundary, after which they are effectively convected a distance d in a random direction depending on which boundary is crossed. Thus, the effective diffusion coefficient for the random walk is

$$D^* = f d^2 \tau_H^{-1},$$

where f is the fraction of particles in the boundary layer, d is the step size, and τ_H a roll circulation time. To estimate f we note that it is specified by the number of particles close enough to the roll boundary to diffuse to the neighboring roll in a circulation time. Thus, $f = \delta/d$ with the boundary layer thickness specified by $\delta^2 = D\tau_H$. This leads to an estimate for the effective diffusion coefficient

$$D^* \approx (D\tilde{u}d\beta)^{1/2}, \tag{5}$$

which will be verified from our mathematical discussion.

To pose the mathematical problem, we observe that we seek a steady-state solution of the form

$$n(x,y) = \bar{n}_0' x + n_p(x,y),$$

where $n_p(x,y)$ is a periodic function with periods $2d$ in x and $2d/\beta$ in y. Now, using Eqs. (2) and (3) we have

$$\hat{\mathbf{x}} \cdot \mathbf{u}(x,y) = -\hat{\mathbf{x}} \cdot \mathbf{u}(-x,y), \qquad \hat{\mathbf{x}} \cdot \mathbf{u}(x,y) = \hat{\mathbf{x}} \cdot \mathbf{u}(x,-y)$$

$$\hat{\mathbf{y}} \cdot \mathbf{u}(x,y) = \hat{\mathbf{y}} \cdot \mathbf{u}(-x,y), \qquad \hat{\mathbf{y}} \cdot \mathbf{u}(x,y) = -\hat{\mathbf{y}} \cdot \mathbf{u}(x,-y).$$

Then, if we consider the mirror inversions of Eq. (1) about the $x = 0$ and the $y = 0$ planes, the following exact relations, compatible with our desired solution, is admitted,

$$\frac{\partial n}{\partial x}(x,y) = \frac{\partial n}{\partial x}(-x,y), \qquad \frac{\partial n}{\partial y}(x,y) = \frac{-\partial n}{\partial y}(x,-y).$$

Now, sufficiently inside the cell boundaries, Eq. (1) admits the asymptotic solution for large Peclet number

$$n(x,y) = n\left(\frac{d}{2}, \frac{d}{2\beta}\right), \qquad \begin{array}{l} 0 < x < d, \\ 0 < y < d/\beta, \end{array}$$

with $n(x,y)$ changing by $\bar{n}_0' d$ from cell to cell in the x-direction. Now, using $\frac{\partial n}{\partial x}(x,y) = \frac{\partial n}{\partial x}(-x,y)$, we have

$$d\bar{n}_0' = n\left(\frac{d}{2}, y\right) - n\left(-\frac{d}{2}, y\right) = \int_{-d/2}^{d/2} dx \frac{\partial n}{\partial x}(x,y)$$

$$= 2\int_0^{d/2} dx \frac{\partial n}{\partial x}(x,y).$$

It then follows that

$$n(0,y) = n\left(\frac{d}{2}, y\right) - \int_0^{d/2} dx \frac{\partial n}{\partial x}(x,y)$$

$$= n\left(\frac{d}{2}, \frac{d}{2\beta}\right) - \frac{d}{2}\bar{n}_0' \qquad \text{(independent of } y\text{)}.$$

Similarly, we find

$$n(d,y) = n\left(\frac{d}{2}, \frac{d}{2\beta}\right) + \frac{d}{2}\bar{n}_0'.$$

The condition $\frac{\partial n}{\partial y}(x,y) = -\frac{\partial n}{\partial y}(x,-y)$ demands

$$\frac{\partial n}{\partial y}(0,y) = 0.$$

Further, one finds $\frac{\partial n}{\partial y}(d,y) = 0$ if one imposes the y-periodicity condition together with mirror symmetry about the $y = 0$ plane.

We also note that these conditions are correct independent of Peclet number if it can be shown that there is one x = constant plane on which n is a constant. Such a plane exists in a steady-state problem where $n(x,y)$ is specified to be zero on one x-boundary.

Thus we have justified seeking a solution within a single cell $d > x > 0$, $d/\beta > y > 0$. The boundary conditions are

$$\tilde{n} = \frac{1}{2}\bar{n}_0' d \qquad \text{at} \qquad x = d, \tag{6a}$$

$$\tilde{n} = -\frac{1}{2}\bar{n}_0' d \qquad \text{at} \qquad x = 0, \tag{6b}$$

$$\frac{\partial \tilde{n}}{\partial y} = 0 \qquad \text{at} \qquad y = 0,\ \frac{d}{\beta}, \tag{6c}$$

where $\tilde{n} = n - n_0$. From such a steady-state solution the flux across the roll and hence, the effective diffusion coefficient D^* may be calculated. Thus our equation is

$$\nabla \cdot \mathbf{u}\tilde{n} = D\nabla^2 \tilde{n} \tag{7}$$

in the domain d, $d/\beta > x$, $y > 0$ subject to boundary conditions (6), and $\mathbf{u}$ specified by Eq. (2).

For the sake of completeness and comparison with later numerical work, we first provide a derivation for the simple case of small Peclet number by expanding Eq. (7) in powers of $1/D$. We then find $n_0 = \bar{n}_0' x$,

$$n_1 = d^2 \beta \tilde{u} \bar{n}_0' \sin \pi \frac{x}{d} \cos \pi \frac{\beta y}{d} \Big/ \pi^2 \left(1 + \beta^2\right) D$$

from which we can immediately compute the volume-averaged convective flux $u_x n_1$ and find for the effective diffusion coefficient at small Peclet number

$$D^* = D + \frac{\beta^2 \tilde{u}^2 d^2}{4\pi^2 (1+\beta^2) D}. \tag{8}$$

To show that the volume-average of nu_x is the exact flux, we note that at fixed x,

$$\bar{F} = -\int_0^{d/\beta} dy D \frac{\partial \tilde{n}}{\partial x} + \int_0^{d/\beta} dy \tilde{n} u_x \equiv (D^* - D)\, \bar{n}_0' \frac{d}{\beta}$$

is independent of x. Averaging over x then gives

$$(D^* - D)\, \bar{n}_0' = \frac{\beta}{d^2} \int dx\, dy \tilde{n} u_x.$$

Returning to the case of large Peclet number, we are interested in the limit of slow diffusion where the convection along streamlines is very rapid, and we need only consider diffusion across streamlines. To that end it is useful to use the streamline function ψ and an orthogonal angle-like coordinate θ as the variables in which to solve the problem. While it is possible to write down θ explicitly in terms of x and y, this will turn out not to be necessary for our purposes. Making the standard coordinate transformation of the Laplacian, Eq. (7) becomes

$$\frac{\partial}{\partial \theta} \frac{|u| \tilde{n}}{|\nabla \psi|} = \frac{\tilde{u} d}{\pi} \frac{\partial \tilde{n}}{\partial \theta} = D \frac{\partial}{\partial \psi} \frac{|\nabla \psi|}{|\nabla \theta|} \frac{\partial \tilde{n}}{\partial \psi}.$$

Here we have used Eq. (2) and have omitted the diffusion along streamlines. We may thus write

$$\frac{\partial \tilde{n}}{\partial \theta} = D' \frac{\partial}{\partial \psi} \frac{|\nabla \psi|}{|\nabla \theta|} \frac{\partial \tilde{n}}{\partial \psi}, \tag{9}$$

where $D' \equiv \pi D / \tilde{u} d \ll 1$ in our large Peclet number limit. Thus, solutions to Eq. (9) will exponentiate rapidly in ψ and we may expect $\tilde{n}$ to be confined to a small boundary layer near $\psi = 0$. Similarly, we may neglect the weak ψ variation of the geometric factors $|\nabla \psi| / |\nabla \theta|$, use their values at $\psi = 0$ to define a new angle variable

$$\theta^* = \frac{\int_0^{\ell} |\nabla \psi| dl'}{\oint |\nabla \psi| dl'},$$

where the indicated streamline integrals are to be taken along the boundary of the roll. θ^* changes by unity in passing completely around the roll. In these variables our equation becomes

$$\frac{\partial \tilde{n}}{\partial \theta^*} = D'' \frac{\partial^2 \tilde{n}}{\partial \psi^2} \tag{10}$$

with $D'' \equiv D' \oint |\nabla\psi| dl \equiv \frac{\pi D}{\bar{u} d} \oint |\nabla\psi| dl$. We note that Eq. (10) implies a boundary layer thickness $\delta\psi \sim (D'')^{1/2}$ as estimated earlier. Using Eq. (3), we may now map out the roll boundaries as expressed in θ^*. First we note that the complete circuit integral

$$\oint |\nabla\psi| dl' = 4\left(\beta + \frac{1}{\beta}\right). \tag{11}$$

Further, the boundary $x = 0$, $d/\beta > y > 0$ maps into the range $\left[2\left(\beta^2+1\right)\right]^{-1} > \theta^* > 0$ where θ^* is given by

$$\theta^* = \frac{(1 - \cos \pi\beta y/d)}{4\left(\beta^2+1\right)}, \tag{12}$$

and similar expressions can easily be derived for the other boundaries. We may now define our problem, re-expressing the boundary conditions (6) in the new coordinates as being the solution of Eq. (10) subject to periodicity in θ^* with period 1 and satisfying at $\psi = 0$.

$$\tilde{n} \equiv -\frac{1}{2}\bar{n}_0' d \qquad \text{for} \qquad \frac{1}{2\left(\beta^2+1\right)} > \theta^* > 0, \tag{13a}$$

$$\frac{\partial \tilde{n}}{\partial \psi} = 0 \qquad \text{for} \qquad \frac{1}{2} > \theta^* > \frac{1}{2\left(\beta^2+1\right)}, \tag{13b}$$

$$\tilde{n} = \frac{1}{2}\bar{n}_0' d \qquad \text{for} \qquad \frac{1}{2} + \frac{1}{2\left(\beta^2+1\right)} > \theta^* > \frac{1}{2}, \tag{13c}$$

$$\frac{\partial \tilde{n}}{\partial \psi} = 0 \qquad \text{for} \qquad 1 > \theta^* > \frac{1}{2} + \frac{1}{2\left(\beta^2+1\right)}. \tag{13d}$$

This is still a difficult problem because of the mixed boundary conditions. We note, however, that because of the smallness of D'', the regular solutions must die away rapidly for $\psi > 0$ so that effectively we can take the range of ψ from 0 to ∞. Similarly, as long as we preserve the periodicity of the solution we may let θ^* run from $-\infty$ to ∞, so we are really dealing with a half-space problem. We may convert it to a problem in the complete θ^*, ψ plane, amenable to Fourier transform solution, by the artifice of introducing a source $S(\theta^*)\delta(\psi)$ at the boundary $\psi = 0$ and seeking solutions with $\tilde{n}(\psi) = \tilde{n}(-\psi)$. This artificial source can then be related to the particle flux as will be seen below. Our even solution

will thus have $\partial n/\partial\psi$ change signs at $\psi = 0$. Note that this actually corresponds to $\partial n/\partial x$ being continuous when passing to the next cell.

Thus, we repose Eq. (10) in the full θ^*, ψ plane as

$$\frac{\partial \tilde{n}}{\partial \theta^*} = D'' \frac{\partial^2 \tilde{n}}{\partial \psi^2} + S(\theta^*)\delta(\psi). \tag{14}$$

Here S must have the following properties

$$S\left(\theta^* + \frac{m}{2}\right) = (-1)^m S(\theta^*) \tag{15}$$

with m any integer. This will guarantee the proper periodicity, and imply $\tilde{n}\left(\theta^* + \frac{m}{2}\right) = (-1)^m \tilde{n}(\theta^*)$ as desired. Moreover, $S = 0$ when

$$\frac{1}{2} > \theta^* > \frac{1}{2\left(\beta^2 + 1\right)}. \tag{16}$$

This will satisfy Eq. (13b) since any regular solution to Eq. (14) must be even in ψ, and $\partial n/\partial\psi$ is continuous if $S = 0$. S must now be determined to be compatible with the specified values of n given in Eq. (13a). From Eq. (14) we must have

$$D'' \frac{\partial \tilde{n}}{\partial \psi}\Big|_{\psi=0} = -\frac{S(\theta^*)}{2}. \tag{17}$$

Hence, $S(\theta^*)/2$ is basically the desired flux.

We proceed to Fourier transform Eq. (14) in ψ.

$$\frac{\partial \tilde{n}_k}{\partial \theta^*} = -D'' k^2 \tilde{n}_k + S(\theta^*)$$

with solution

$$\tilde{n}_k = \int_{-\infty}^{\theta} e^{-D'' k^2 (\theta^* - \theta^{*'})} S\left(\theta^{*'}\right) d\theta^{*'}. \tag{18}$$

Using Eq. (15), we may convert this solution to one expressed in the finite range $\left[2\left(\beta^2+1\right)\right]^{-1} > \theta^* > 0$

$$\tilde{n}_k = \int_0^{\theta^*} e^{-D'' k^2 (\theta^* - \theta^{*'})} S\left(\theta^{*'}\right) d\theta^{*'}$$

$$+ \int_0^{\left[2(\beta^2+1)\right]^{-1}} e^{-D'' k^2 (\theta^* - \theta^{*'})} \left[-e^{-\frac{D'' k^2}{2}} + e^{-D'' k^2} - e^{-3\frac{D'' k^2}{2}} + \ldots\right] S\left(\theta^{*'}\right) d\theta^{*'}.$$

Finally we invert the transform to find the density $\tilde{n}$ at $\psi = 0$ in the range $\left[2\left(\beta^2+1\right)\right]^{-1} > \theta^* > 0$

$$\tilde{n}(\theta^*) \equiv -\frac{1}{2}\bar{n}_0' d$$

$$= \frac{1}{2\sqrt{\pi D''}}\left[\int_0^{\theta^*} \frac{S\left(\theta^{*'}\right) d\theta^{*'}}{\sqrt{\theta^* - \theta^{*'}}} + \sum_{m=1}^{\infty}(-1)^m \int_0^{\left[2(\beta^2+1)\right]^{-1}} \frac{S\left(\theta^{*'}\right) d\theta^{*'}}{\sqrt{m/2 + (\theta^* - \theta^{*'})}}\right]. \tag{19}$$

We have thus converted our complex boundary value problem to an integral equation over a finite interval. This equation is exact in the large P limit. This could be solved numerically or, by Fourier transform, converted to a symmetric matrix equation from which a variational expression for the flux could be obtained. However, since physically we expect that the first term in the above integral equation corresponding to local contributions will dominate except for very small β, and further, since the second term is slowly varying in θ, we choose to find an approximate solution by using an expansion in θ for the kernel of the second term. Note that for large β, corresponding to many experiments, this should, in particular, be an excellent approximation. Our results will tend to verify the approximation since the local contributions indeed dominate. We thus use the expansion

$$\sum_{m=1}^{\infty}(-1)^m \frac{1}{\sqrt{m/2 + (\theta^* - \theta^{*'})}} = \sqrt{2}\sum(-1)^m \left[m + 2\left(\theta^* - \theta^{*'}\right)\right]^{-1/2}$$

$$= \sqrt{2}\sum\left[(-1)^m (m)^{-1/2} - \left(\theta^* - \theta^{*'}\right) m^{-3/2} + \ldots\right]$$

$$= -\sqrt{2}\Big\{\left(1 - \sqrt{2}\right)\xi\left(\frac{1}{2}\right)$$

$$- \left(1 - \frac{1}{\sqrt{2}}\right)\xi\left(\frac{3}{2}\right)\left(\theta^* - \theta^{*'}\right)\ldots\Big\},$$

where $\xi(1/2)$, $\xi(3/2)$ are the Riemann Zeta Functions. Hence, we approximate

$$\sum(-1)^m \frac{1}{\sqrt{m/2 + (\theta^* - \theta^{*'})}} = -.86 + 1.08\left(\theta^* - \theta'^*\right).$$

Note that $\max\left|\theta^* - \theta^{*'}\right| = \left[2\left(\beta^2+1\right)\right]^{-1}$ so that except for small β, the kernel does not vary rapidly. We will see later that even for $\beta \to 0$ quite accurate results are obtained

from the truncation. With this truncation we must solve Eq. (19) in the form

$$-\sqrt{\pi D''}\bar{n}_0' d = \int_0^{\theta} \frac{S\left(\theta^{*'}\right) d\theta^{*'}}{\sqrt{\theta^* - \theta^{*'}}} - \left[\int_0^{[2(\beta^2+1)]^{-1}} S\left(\theta_*'\right)\left\{\left[.86 + 1.08\theta^{*'}\right] - 1.08\theta^*\right\} d\theta^{*'}\right]. \tag{20}$$

This equation is easily solved by Laplace Transform if we extend the domain of this equation to $0 < \theta^* < \infty$ with only the solution in the region $0 < \theta^* < \left[2\left(1+\beta^2\right)\right]^{-1}$ being physical. Introducing the Laplace Transform variable p and using the Faltung Theorem,

$$\sqrt{\pi}\frac{S(p)}{\sqrt{p}} = \frac{1}{p}\left[-\sqrt{\pi D''}\bar{n}_0' d + \int_0^{[2(\beta^2+1)]^{-1}} S\left(\theta^{*'}\right)\left[.86 + 1.08\theta^{*'}\right] d\theta^{*'}\right] - \frac{1.08}{p^2}\int_0^{[2(\beta^2+1)]^{-1}} S\left(\theta^{*'}\right) d\theta^{*'},$$

or inverting the transform

$$S(\theta^*) = \frac{1}{\pi}\left\{\theta^{*-1/2}\left[-\sqrt{\pi D''}\bar{n}_0' d + \int_0^{[2(\beta^2+1)]^{-1}} S\left(\theta^{*'}\right)\left[.86 + 1.08\theta'^*\right] d\theta^{*'}\right] - \theta^{*1/2} 2.16 \int_0^{[2(\beta^2+1)]^{-1}} S\left(\theta'^*\right) d\theta'^*\right\}.$$

By substituting the form

$$S(\theta^*) = -\sqrt{\pi D''}\bar{n}_0' d\left[a\theta^{*-1/2} - b\theta^{*1/2}\right] \tag{21}$$

into the integrals, we may match coefficients and obtain

$$\begin{aligned} a &= \left[\pi - \frac{(1.22 - .20\lambda)}{(\beta^2+1)^{1/2}} - \frac{(.25 - .07\lambda)}{(\beta^2+1)^{3/2}}\right]^{-1} \\ \lambda &= \left[\left(\beta^2+1\right)^{3/2} + .16\right]^{-1} \\ b &= .97\left(\beta^2+1\right)\lambda a. \end{aligned} \tag{22}$$

It can be seen that the corrections obtained to the simple approximation of keeping the first term in (20) are finite, but numerically small even for $\beta = 0$. We may now construct

the flux $F(y)$, across the $x = 0$ boundary which is the physical quantity of interest. Using Eqs. (3), (11), and (17) we have

$$F(y) = -D(\nabla\psi)\frac{\partial\tilde{n}}{\partial\psi} = (\nabla\psi)\frac{S}{2D''}D = \sin\frac{\pi\beta y}{d}S(\theta^*)\frac{\tilde{u}\beta}{8\,(1+\beta^2)}.$$

Then expressing the answer in terms of y by using Eq. (12),

$$\theta^{*1/2} = \frac{1}{\sqrt{2}}\frac{1}{(\beta^2+1)^{1/2}}\sin\frac{\pi\beta y}{2d},$$

we find that the flux crossing the surface $x = 0$ is

$$F(y) = -\pi\sqrt{\frac{D\tilde{u}d\beta}{2}}\cos\frac{\pi\beta y}{2d}a(\beta)\left[1 - .48\lambda(\beta)\sin^2\frac{\pi\beta y}{2d}\right]\bar{n}_0', \tag{23}$$

where a and λ have been defined in Eq. (22). The flux is thus a maximum at $y = 0$ where the flows in the x-direction enter the corner and falls to zero at the corner where the x flows diverge. Finally we may average the flux over the period $y = 0$ to d/β to obtain the effective diffusion coefficient

$$D^* = \frac{\beta\int_0^{d/\beta}dyF(y)}{d} = \sqrt{2D\tilde{u}d\beta}a[1 - .16\lambda]. \tag{24}$$

We have, of course, defined D^* such that the y-averaged global flux $\bar{F} = -D^*\bar{n}_0'$. We may note that the aspect ratio dependence enters primarily through the factor $\sqrt{\beta}$ since $a[1 - .16\lambda]$ varies only from .45 at $\beta = 0$ to .32 at $\beta = \infty$. Aside from this aspect ratio dependence, the diffusion coefficient is exactly of the form given by our earlier physical argument leading to Eq. (5).

We may check the accuracy of our expansion of the kernel by looking at the limit $\beta = 0$ where it is least justified. In this limit we know $\tilde{n}$ at all points on the boundary since the boundary consists only of the boundaries at $x = 0$, d, and $\tilde{n} = -(-1)^m\bar{n}_0'/2$ where $m/2 - 1/2 > \theta^* > m/2$. Hence, we may use Eq. (18) directly to find by inverting the Fourier transform

$$\pm\frac{d}{2}\bar{n}_0' = \frac{1}{2\sqrt{\pi D''}}\int_{-\infty}^{\theta^*}\frac{S\left(\theta^{*'}\right)d\theta^{*'}}{\sqrt{\theta^* - \theta^{*'}}}\begin{cases} - \text{ sign if } 2\theta^* \bmod (2) < 1 \\ + \text{ sign if } 2\theta^* \bmod (2) > 1. \end{cases}$$

This may now be solved exactly by Laplace transform to yield for $1/2 > \theta^* > 0$

$$S(\theta^*) = -2\frac{\sqrt{\pi D''}}{\pi}\sum_{m=0}^{\infty}(-1)^m\frac{d}{\sqrt{m/2+\theta^*}}\bar{n}_0'. \tag{25}$$

In order to compare the total flux with our previous estimate we need to calculate

$$\int S(\theta^*)d\theta^* = \frac{2d}{\pi}\sqrt{\pi D''}\bar{n}_0' \times \left[4\left(2-2^{-1/2}\right)\xi\left(-\frac{1}{2}\right)\right] = -\sqrt{\pi D''}\bar{n}_0' d \times .696 \ .$$

Our approximation, on the other hand, yielded from Eq. (21)

$$\int S(\theta^*)d\theta^* = -\sqrt{\pi D''}\bar{n}_0' d\left[\sqrt{2}a - \sqrt{2}\frac{b}{6}\right] = -\sqrt{\pi D''}\bar{n}_0' d \times .64 \ .$$

We may thus conclude that our approximate expansion of the kernel yields a good representation of the solution for all β. In order to obtain a highly accurate value of the flux for arbitrary β we have carried the expansion of the kernel in Eq. (19) to higher order, the integrals being readily done in terms of Riemann Zeta functions and an expansion for $S(\theta^*)$ in inverse powers of (β^2+1) developed by the method shown above. The resulting diffusion coefficient is given by

$$D^* = \frac{(2D\tilde{u}d\beta)^{1/2}}{\pi A(Z)}, \tag{26}$$

where with $Z \equiv (\beta^2+1)^{-1}$,

$$A(Z) = 1 - .384Z^{1/2} + .081Z^{3/2} - .060Z^{5/2} + .011Z^3 + .033Z^{7/2} - .008Z^4 - .028Z^{9/2} + (.012Z^5) \ . \tag{27}$$

The expansion was carried out to order $Z^{9/2}$ and the last term in parenthesis arbitrarily added to agree with Eq. (25) for $Z = 1$ which can be put in the form $A(1) = -\left[(8\sqrt{2}-4)\zeta(-1/2)\right]^{-1} = .657$. It can be seen that Eqs. (26) and (27) should be accurate to within a small fraction of a percent over the entire range of β. A simple approximation to Eq. (27) correct for $Z = 1$ and $Z = \infty$ can be given by

$$A(Z) = 1 - .343Z^{1/2}, \tag{28}$$

which is in error by about a percent for the case of a square cell, $Z = .5$. Equation (27) yields $A(.5) = .749$.

Further we note that, if desired, one could use our solution (21) to calculate the density along the boundary $y = d/\beta$ by using Eq. (19) in the domain $1/2 > \theta^* > \left[2\left(\beta^2+1\right)\right]^{-1}$,

$$\tilde{n}(\theta^*) = \frac{1}{2\sqrt{\pi D''}}\sum_{m=0}^{\infty}(-1)^m \int_0^{[2(\beta^2+1)]^{-1}} \frac{S\left(\theta^{*'}\right)d\theta^{*'}}{\sqrt{m/2+(\theta^*-\theta^{*'})}}.$$

If for simplicity we use Eq. (21) neglecting the small b term we find

$$\tilde{n}(\theta^*) = -a\bar{n}_0' \sum_{m=0}^{\infty} (-1)^m \sin^{-1}\left[\left(\beta^2+1\right)(m+2\theta^*)\right]^{-1/2}. \tag{29}$$

We note that for large and moderate β, $\tilde{n}$ becomes small $\tilde{n} \sim -.39/\left(\beta^2+1\right)^{1/2} d\bar{n}_0'/2$ as θ^* approaches $1/2$. It does not change sign and thus a discontinuity appears at the corner $\theta^* = 1/2$. This, however, is physically acceptable since the discontinuity has a zero width in ψ. In fact, right at the corners where the velocity vanishes, the diffusion along streamlines should be taken into account and a small smoothing in θ^* over a distance $\sqrt{D''}$ must occur. This sub-boundary cannot, however, affect our results to the dominant order to which we calculate.

To indicate again the physical nature of the solution, we show in Fig. 2 a schematic plot of the density versus x for fixed y. The solid curve would apply for all y except the horizontal boundaries, the dotted curve would apply at the boundaries ($y = 0$ or d/β).

The main point, of course, is that the density must be flat in the interior of the rolls due to the rapid circulation so that the global gradient must appear as a steep gradient confined to the boundary layer. This steep gradient then leads to an enhanced diffusive flux as given by Eq. (26).

III. GENERALIZATION TO ARBITRARY PERIODIC FLOW PATTERNS

We now further note that our calculation is not limited to the particular streamline function assumed in Eq. (3). A typical situation might involve unstable rolls developing from an equilibrium homogeneous in x but with structure in y. To describe such a case we choose a streamline function

$$\psi = \sin\frac{\pi x}{d} f\left(\pi\beta\frac{y}{d}\right), \tag{30}$$

where $f(0) = f(\pi) = 0$ to define the streamline boundaries as being at $y = 0$, d/β and further, we normalize $f(\pi/2) = 1$ so that $\tilde{u}$ retains its meaning as the peak velocity along the vertical ($x = 0$) boundary. It is also assumed that $f(\pi\beta y/d) = f\left[\pi(1-\beta y/d)\right]$.

A particular case of interest is that of rough (rigid) horizontal boundaries at $y = 0$, d/β. For that case, since the horizontal velocity must vanish at the rough wall, it follows that $f'(0) = f'(\pi) = 0$. While this leads to a vanishing of the geometric factor $|\nabla\psi|/|\nabla\theta|$

in Eq. (8) along the horizontal boundary, we will show below that this does not invalidate our results to leading order in large Peclet number.

We indicate here the modifications in our calculation introduced by the change in streamline function neglecting for the moment any possible singular behavior. Equation (10) remains valid as do the definitions

$$D'' \equiv \frac{\pi D}{\tilde{u} d} \oint |\nabla \psi| dl \qquad \text{and} \qquad \theta^* \equiv \frac{\int_0^\ell |\nabla \psi| dl}{\oint |\nabla \psi| dl}$$

with the integrals taken along streamline boundaries as before. Hence, the governing equation (19) is recovered except that the upper limit of the last term which has been defined to be

$$\frac{1}{2} \frac{\int |\partial \psi / dx| dy}{\int |\partial \psi / dx| dy + \int |\partial \psi / \partial y| dx}$$

now becomes

$$\frac{Z}{2} = \frac{1}{2} \frac{\int_0^\pi f(\mu) d\mu}{\int_0^\pi f(\mu) d\mu + 2\beta^2 f'(0)} \tag{31}$$

and

$$D'' = \frac{2\pi D}{\tilde{u} d\beta} \left[\int_0^\pi f(\mu) d\mu + 2\beta^2 f'(0) \right]. \tag{32}$$

Our previous solution, Eq. (21), now applies with $\left(\beta^2 + 1\right)^{-1}$ replaced by Z in Eq. (22). Note that $Z = 1$ for the rough boundary case, since the vanishing of f' implies that the total range of θ^* is subsumed on the vertical boundaries. We may now calculate the desired diffusivity

$$\begin{aligned} D^* = -\frac{D}{\bar{n}_0'} \frac{\int_0^{d/\beta} \frac{\partial \tilde{n}_0}{\partial x} dy}{d/\beta} &= -\frac{D\beta}{d\bar{n}_0'} \frac{\pi}{d} \int_0^{d/\beta} \frac{\partial \tilde{n}}{\partial \psi} f\left(\frac{\pi \beta y}{d}\right) dy \\ &= -\frac{D\beta}{d\bar{n}_0'} \frac{\pi}{d} \int_0^{d/\beta} \frac{S}{2D''} f\left(\frac{\pi \beta y}{d}\right) dy \\ &= -\frac{D\beta}{2d\bar{n}_0'} \frac{\oint |\nabla \psi| dl}{D''} \int_0^{Z/2} S\left(\theta^*\right) d\theta^* \\ &= -\frac{\tilde{u} d\beta}{2\pi} \frac{1}{d\bar{n}_0'} \int_0^{Z/2} S\left(\theta^*\right) d\theta^*. \end{aligned}$$

Therefore,

$$D^* = \frac{\tilde{u}d\beta}{2\sqrt{\pi}}\sqrt{D''}g(Z),$$

where $g(Z)$ is determined from the same integrals as those leading to Eqs. (22) or (27). Finally then

$$D^* = \left[D\tilde{u}d\beta \int_0^\pi f(u)du\right]^{1/2} \Big/ \pi A(Z), \tag{33}$$

where Z has been defined in Eq. (31) and $A(Z)$ in Eq. (27). This provides our large Peclet number diffusivity for the general stream function. For the rough boundary case $Z = 1$ and

$$D^* = .48\left[D\tilde{u}d\beta \int_0^\pi f(u)du\right]^{1/2}. \tag{34}$$

We now discuss the physics of the rough boundary case. We have seen that $\nabla\psi/\nabla\theta$ vanishes near the horizontal boundaries, in fact vanishing like $y \sim \psi^{1/2}$. Hence, since $\psi \sim D^{1/2}$, these terms are small by order $D^{1/4}$ compared to those we have kept. Thus, we have neglected cross-field diffusion near $y = 0$.

To understand the situation physically we revert to the arguments given at the beginning of this article. The particles that undergo mixing between cells lie within a vertical width Δx of the cell boundary that is determined from the condition that cross stream diffusion is balanced by the vertical convection time $\tau_H \approx d/\beta\tilde{u}$. Therefore,

$$\Delta x^2 \approx D\tau_H = Dd/\beta\tilde{u}.$$

The particles in the boundary layer will take a random step d in a crossing time τ_c. Hence, the effective diffusion coefficient is given by

$$\Delta x^2 = fd^2/\tau_c,$$

where f is the fraction of particles in the boundary layer. Now f is estimated as $\beta\Delta y/d$, where Δy is related to Δx by the condition that $\Delta\psi$ along the vertical and horizontal boundaries be the same. Thus, $\beta^2\Delta y^2 \simeq \Delta x d$. The crossing time for particles that are Δy

from the horizontal boundaries is $\tau_c \approx d/\left(\beta^2 \tilde{u} \Delta y/d\right)$. We then find

$$f = \frac{\beta \Delta y}{d} \approx \left(\frac{\Delta x}{d}\right)^{1/2} \approx \left(\frac{D}{\beta \tilde{u} d}\right)^{1/4}$$

$$\frac{1}{\tau_c} \approx \frac{\beta^2 \tilde{u} \Delta y}{d^2} \approx \frac{\beta \tilde{u}}{d}\left(\frac{\Delta x}{d}\right)^{1/2} \approx \frac{\beta \tilde{u}}{d}\left(\frac{D}{\beta \tilde{u} d}\right)^{1/4}$$

$$D^* \approx d^2 f/\tau_c \approx (\beta \tilde{u} d D)^{1/2},$$

as given by Eq. (34).

However, for particles very close to the boundary, the cross-field diffusion must be considered and an "inner" boundary layer will form. For a particle very near $y = 0$, $\Delta y \sim (D\tau_c)^{1/2}$ and since $\tau_c \sim 1/u_x$ and $u_x \sim \Delta y$, we find $\Delta y \sim D^{1/3}$. As before, the diffusivity is $D^* \sim f/\tau_c$, and with $f \sim \Delta y$, we find $D^* \sim D^{2/3}$. This is a smaller contribution to D^* than previously calculated since $D^{1/3} < D^{1/4}$ and the inner boundary layer contribution may be neglected asymptotically. Needless to say, one might anticipate that our results might only be an accurate approximation for very large Peclet numbers. In fact, since $\left(D^{1/3}\right)$ of the particles in the boundary layer are being improperly calculated, we would expect a diffusivity of the form $D^* \sim aD^{1/2} + bD^{2/3}$ of which we have calculated the first term.

Finally, we note that the method of calculation can be generalized even further to describe diffusion in even more general periodic flow structures such as the forced rotating cylinder problem posed in Ref. 15. The description of the problem and the analytic solution is given in the appendix. The numerical result given in Ref. 15 is recovered.

IV. MEASUREMENTS OF THE DIFFUSION COEFFICIENT

Simulations of the diffusive convective flow given by Eqs. (1)–(3) are made by following particles along their laminar flow lines and simultaneously introducing periodic random displacements after each small time interval τ_K. The particles move according to the equations:

$$\dot{x} = -\partial_y \Psi(x,y) \tag{35}$$

$$\dot{y} = \partial_x \Psi(x,y),$$

where we now choose $\Psi(x,y) = \sin x \cos y$. Note that $\omega_b = 1$, where ω_b is the angular frequency of rotation around the elliptic fixed points, and the size of the square cell ($\beta = 1$) is π. During the random jump a particle moves from $\mathbf{x}$ to $\mathbf{x}+\boldsymbol{\xi}$ with a probability given by $W(\xi_x, \xi_y)$. Thus, the change of a given particle distribution in a time τ_K due to the random scattering in and out of a volume element surrounding $\mathbf{x}$ is given by:

$$f(\mathbf{x}, t+\tau_K) - f(\mathbf{x},t) = \int d\boldsymbol{\xi} W(\boldsymbol{\xi}) f(\mathbf{x}-\boldsymbol{\xi}, t) - f(\mathbf{x},t) \int d\boldsymbol{\xi} W(\boldsymbol{\xi}). \tag{36}$$

We studied two different probabilities $W(\boldsymbol{\xi})$:

a) Constant $\boldsymbol{\xi}$ steps

$$W(\boldsymbol{\xi}) = \frac{1}{4}\left[\delta(\xi_x - l) + \delta(\xi_x + l)\right]\left[\delta(\xi_y - l) + \delta(\xi_y + l)\right], \tag{37}$$

for which $D = l^2/2\tau$.

b) Gaussian distribution of steps

$$W(\boldsymbol{\xi}) = \left(2\pi \left\langle \xi^2 \right\rangle\right)^{-1/2} \exp\left(-\frac{\xi^2}{2\left\langle \xi^2 \right\rangle}\right) \tag{38}$$

for which $D = \left\langle \xi^2 \right\rangle / 2\tau$.

For an ensemble of N particles the evolution of the system is computed according to Eq. (35). A sixth order Runge-Kutta method is used to integrate the equations of motion between random kicks. The time step is chosen internally with the requirement that the overall estimated error at the end of the integration be less than a specified value (typically

10^{-6}). In the stochastic part of the evolution, the particles are randomly displaced in both the x and y direction. The system is allowed to evolve for several rotation periods until the transients decay away, and then measurements are taken at regular intervals of $n\tau_K$, with $n \sim 50 - 1000$ in different runs. Two initial distributions are used:

$$\begin{aligned} &1) \quad f(x,y,t_0) = \text{const.} \qquad \text{for} \qquad |x| < x_0, \quad |y| < y_0 \\ &2) \quad f(x,y,t_0) = \delta(x - x_0), \qquad |y| < y_0 \end{aligned} \tag{39}$$

and no effect of the shape of $f(x,y,t_0)$ or the values of x_0 and y_0 is detected in the results other than the length of time required for the transients to die out.

Two methods are used to obtain values of the effective diffusion coefficient D^*. In the first method we follow the evolution of the given initial distribution. This initial value method relies on the fact that, since the evolution of the system is equivalent to a diffusion process with an effective diffusion coefficient D^*, the particle distribution function $f(x,y,t)$ will, after an initial transient, have a Gaussian profile with a standard deviation σ^2 related to the running diffusion coefficient $D^*(t)$ by

$$\sigma_x^2(t) = \frac{1}{N}\sum_{i=1}^{N}\left(x_i(t) - \langle x(t)\rangle\right)^2 = 2D^*(t)t \tag{40}$$

with D^* given by

$$D^* = \lim_{t \gg \tau} D^*(t).$$

Three different values of kick length were used, $.01\pi$, $.05\pi$, and $.1\pi$ (the size of the cell is π). In each case the kick length l was chosen so that $l \ll \min(\delta, \pi)$, where $\delta^2 = D\tau_H$ is the boundary layer thickness (cf. Sec. II). The need to make ℓ small enough is essential for an accurate simulation.

To insure that the codes were working properly, the system was first advanced only with random kicks (no laminar motion) and the value of D^* obtained was found to agree with the theoretical value $D^* = \ell^2/2\tau_k$ to well within the error bars. Also for pure laminar flow (no kicking), the particles were advanced for 500 rotation periods with no more than the nominal error (typically 10^{-6}) in the final position of the particle.

In the first example shown in Fig. 3, the evolution of the distribution from stochastic kicks with the Gaussian probability distribution $W(\xi)$ (Eq. (38)) is used with a mean step

length $\langle \xi^2 \rangle^{1/2} = 0.1$ and the step period τ_K chosen to give the desired collisional diffusion coefficient D. Figure 3a shows a sample particle distribution in the $x-y$ plane. In this example, 256 particles randomly distributed in the unit cell at the origin are advanced 10^4 random steps, with τ_K chosen to give $D = 0.9$. Figure 3b shows the running diffusion coefficient, $D_x^*(t)$, defined in Eq. (40).

In the initial value method, the system was evolved for typically 20 circulation periods τ_H before any measurements were taken to allow for any transients to die out. Also $D^*(t)$ was calculated at times $4-5\tau_H$ apart to keep the values of $D^*(t)$ statistically independent. These values were then averaged to provide the value of D^*. To make sure that all the values of the running diffusion coefficient $D^*(t)$ used in the calculation of the average diffusion coefficient D^* are statistically independent, the correlation time, τ_c, was computed. The system was advanced according to Eq. (35) and after each kick the two-time correlation function

$$C(t) = \frac{1}{N} \sum_{i=1}^{N} \frac{(x_i(t_0) - \langle x_i(t_0) \rangle)(x_i(t) - \langle x_i(t) \rangle)}{\sigma(t_0)\,\sigma(t)} \tag{41}$$

was calculated. Figure 4 shows a typical plot of $C(t)$; the unit of time is the kick time, τ_K. The time at which the value of $C(t)$ falls to $1/e \simeq .37$ is the correlation time τ_c. In this particular case, $\tau_H = 20\tau_K$.

Since the assumption that the particle distribution function $f(x, y, t)$ is Gaussian is crucial to the initial value measurements, a statistical test, the χ^2 goodness-of-fit test, was used to test $f(x, y, t)$ for normality and reject the values of $D^*(t)$ that were obtained from particle distributions that were not a good approximation to a Gaussian. A 90% confidence level was used. The critical value χ_c^2 for the chosen confidence level is determined from tables, and the test statistic CHI is compared to it. If CHI $< \chi_c^2$, the distribution is a good approximation to a Gaussian, and the value of $D^*(t)$ obtained from it is accepted, whereas if CHI $> \chi_c^2$ it is rejected.[17] The good values of $D^*(t)$ that were obtained in this way were used to calculate the quoted D^* for that particular choice of parameters. The same χ^2 test with a 90% confidence level as before was used to estimate the error bar.

Figure 5 shows D^* as a function of D. A regression fit of the data to the curves

$$\begin{aligned} D^*(D) &= C_1 D^{1/2} \qquad \text{for} \qquad D < 0.5 \\ D^*(D) &= D + C_2/D \qquad \text{for} \qquad D > 0.5 \end{aligned} \tag{42}$$

was used to derive the two solid curves. The regression fits give $C_1 = 1.04 \pm .02$, $C_2 = .12 \pm .03$. These values overlap with the derived asymptotic values $C_1 = 1.065$ (obtained from Eq. (26) using $d = \pi$, $\beta = 1$, $Z(.5) = .7494$) and $C_2 = 1/8$.

A second simulation method was developed that makes use of the analytic theory of Sec. II. The system is considered confined to a domain $-x_0 < x < x_0$, $-\pi/2 < y < \pi/2$ with $x_0 = n\pi$ and n an integer. Beyond this domain, values in y are taken periodic in the basic y-cell. Particles leaving the boundary $x = \pm x_0$ are annihilated (hence there is a sink there) and reintroduced at $x = 0$, $y = (-1)^n y$ (hence there is a source at $x = 0$). Thus, the relationship between sources and sinks given by Eq. (15) is preserved. When the system reaches a steady state, the strength of the sources are obtained by counting the particles passing through $x = \pm x_0$. In practice only the y-integrated source, which corresponds to the total number of particles crossing $x = \pm x_0$, is needed. The particles are initially randomly distributed in the range $-x_0 < x < x_0$, $-\pi/2 < y < \pi/2$. In different simulations, different values of x_0 were used to check the consistency of the method, and no significant dependence on the value of x_0 was found for $1 \leq n \leq 5$.

The effective diffusion coefficient is given by

$$D^* = \frac{\lambda (n\pi)^2}{2N}, \tag{43}$$

where N is the total number of particles in the simulation and λ the total number of particles entering at $x = 0$ per unit time. Equation (43) is readily derived by assuming that the mean density $\bar{n}(x)$ satisfies a steady-state diffusion equation

$$\lambda \delta(x) = -D^* \frac{\partial^2 \bar{n}}{\partial x^2}$$

Note that $\bar{n}$ varies linearly in $|x|$, vanishes at the boundaries, and it is required that $\int_{-x_0}^{x_0} \bar{n} dx = N$.

In the simulation the system is allowed to evolve until all transients die out and a steady state is reached, and then the number of particles leaving the range in a suitably chosen time interval are counted.

Figure 6a shows a plot of the number of particles leaving the range as a function of time. Without laminar flow this method also gives $D = \ell^2/2\tau_k$. In this particular example with $x_0 = 1\pi$, 250 particles were advanced for 7000 random steps, and the measurements were taken after the first 3100 steps. The total number of particles, n, escaping between t and $t + 20\tau$ is plotted against t. In Fig. 6b a histogram of the spread of values of n is fitted to a Gaussian and the same scheme as before is used to obtain error estimates for n and hence D^*. Figure 7 shows D^* against D. In this case $C_1 = 1.03 \pm .03$, $C_2 = .09 \pm .03$.

In comparing the properties of the two codes, we note that both the initial value and the steady-state methods exhibited a sensitivity to the value of the kick length l used. They both converged to the theoretical value of D^* for smaller l but in quite different ways. The initial value method produced values of D^* that oscillated around the theoretical curve for large l and the oscillations were reduced as l was reduced. The steady-state method produced values of D^* consistently lower than the corresponding theoretical value for large l and asymptotically approached the curve as l was reduced. The effect was more pronounced for $x_0 = 1\pi$ than it was for larger values of x_0. The length of integration time required to obtain comparable convergence was roughly 1.5 times longer for the initial value method than for the steady-state method. The statistical deviations of the steady-state method consistently conformed better with a Gaussian statistical model than the deviations in the initial value simulations.

As was mentioned in Sec. II above, the particle distribution is expected to be flat in the interior of the rolls with a steep gradient close to the separatrix. Evidence of this was observed during the numerical simulations. In the early times after we start advancing the particles from their initial position, all particles are confined to the cell they are initially placed in. If we run the χ^2 test on that distribution we will see that it is a good fit to a Gaussian. If we wait a bit longer until the distribution flattens in that cell, and a few particles have leaked to the neighboring cells, the distribution is no longer Gaussian, and we have to wait for enough particles to leak to the neighboring cells for the distribution

to regain its Gaussian shape. It was because of this effect that we had to incorporate the χ^2 test in the measuring process and reject the values of D^* that came from non-Gaussian distributions.

V. CONCLUSIONS

To summarize our conclusions, we have found that in the large Peclet number $\left(P = \frac{\text{cell diffusion time}}{\text{cell circulation time}}\right)$ limit the effective diffusion coefficient for horizontal diffusion through a pattern of steady-state laminar convection cells is given by

$$D^* = 0.6(D\tilde{u}d\beta)^{1/2}\alpha. \tag{49}$$

Here, D is the molecular diffusion coefficient, $\tilde{u}$ the peak vertical convection velocity along the cell boundary, d the horizontal cell extent, and d/β the vertical cell extent. α is a coefficient of about unity (varying less than a factor 2 depending on the details of the problem). For a specific streamline function of the typical form of Eq. (30), a detailed calculation of α is given by Eqs. (31), (32), (33), and (27).

A numerical simulation of particle diffusion for the case $\beta = 1$ verifies the analytic prediction and provides a smooth join for the full range of Peclet numbers.

Acknowledgements

This research was supported by U. S. Department of Energy Contract #DE-FG05-80ET-53088.

APPENDIX: THE PROBLEM OF PERIODIC ROTATING CYLINDERS

We now address the problem formulated by Nadim, Cox, and Brenner, who considered the transport of dye (or heat) in a system with nearly laminar flow driven by periodic rotating cylinders. The configuration is shown in Fig. 8. The dotted boundary cell represents the periodic cell of length d. At each vortex is the axis of a rotating porous cylinder of radius $d(1-\delta)/2$, with $\delta \ll 1$, rotating counter-clockwise with an angular frequency Ω. One can show, in the limit of very high Reynolds number, that over most of the fluid a laminar flow pattern is established, with a separatrix indicated by the dashed curve. Inside the dashed curve (interior region) the flow is clockwise, with the speed near the separatrix being

$$u = \frac{d\Omega}{2} + \mathcal{O}(\delta).$$

Near the vertices of the separatrices the speed varies, and is determined by a solution of the Navier-Stokes equation. However, for the purposes of our calculation we can neglect such variation. Outside the separatrix (external region) the flow moves circularly around each cylinder with a speed $u = d\Omega/2 + \mathcal{O}(\delta)$ (with the exception of a flow boundary layer between oppositely rotating cylinders whose detailed form is unimportant to our calculation).

We take the global density variation to be in the x-direction, with

$$\overline{\frac{\partial n_0}{\partial x}} = n_0'$$

$$\overline{\frac{\partial n_0}{\partial y}} = 0.$$

Using the arbitrariness in the overall density of the dye, we choose the dye density to be zero at the origin. Then, within the square of Fig. 8, $n \to n(\psi_{\max}) = dn_0'/2$ in sectors I′ and IV′, $n \to n(\psi_{\max}) = -dn_0'/2$ in sectors II′ and III′.

In the interior we have labelled near each separatrix, regions I, II, III, and IV as indicated in Fig. 8. On the opposite side of the separatrix we have labelled regions I′, II′, III′, and IV′. From the symmetry of the problem, we note that the matching primed regions have identical density gradients on the separatrix. Thus, the exterior region can also be considered as surrounding a rotating cylinder with a streamline moving cylically from region I′ → IV′ → III′ → II′.

In the large Peclet limit (and large Prandtl number so that the laminar flow approximation holds over most of the Peclet boundary layer), we expect the dye density to be spatially constant except near the separatrix, where the density rapidly changes by $n_0' d/2$ when moving from left to right. Then in the neighborhood of a separatrix we can reduce Eq. 7 to Eq. 10. We again introduce source functions, in this case $S_{\rm int}(\theta^*)$ surrounding the interior region and $S_{\rm ext}(\theta^*)$ surrounding an exterior region. The flow circulates in the clockwise direction in circumventing the interior region and the counter-clockwise direction in circumventing the exterior region.

The equation for the dye density is then

$$\frac{\partial n}{\partial \theta^*} = D'' \frac{\partial^2 n}{\partial \psi^2} + S_{\rm int}(\theta^*)\,\delta(\psi); \qquad \text{interior region} \quad \text{(A-1)}$$

$$\frac{\partial [n - n(\psi_{\max})]}{\partial \theta^*} = D'' \frac{\partial^2 [n - n(\psi_{\max})]}{\partial \psi^2} + S_{\rm ext}(\theta^*)\,\delta(\psi); \qquad \text{exterior region.} \quad \text{(A-2)}$$

The solution on the separatrix in terms of $S(\theta^*)$ can then be obtained in the same manner as was Eq. (19), and we find

$$n_{\rm sep}(\theta^*) = \frac{1}{2(\pi D'')^{1/2}} \int\limits_{\substack{-\infty \\ \text{interior} \\ \text{orbit}}}^{0} \frac{d\theta' S_{\rm int}(\theta')}{(\theta^* - \theta')^{1/2}} \qquad \text{(A-3)}$$

$$n_{\rm sep}(\theta^*) - n(\psi_{\max}) = \frac{1}{2(\pi D'')^{1/2}} \int\limits_{\substack{-\infty \\ \text{exterior} \\ \text{orbit}}}^{0} \frac{d\theta' S_{\rm ext}(\theta')}{(\theta^* - \theta')^{1/2}}. \qquad \text{(A-4)}$$

Since n is continuous on the separatrix, $n_{\rm sep}(\theta^*)$ is the same in (A-3) and (A-4). We eliminate $n_{\rm sep}(\theta^*)$ by subtracting the two solutions and find

$$n(\psi_{\max}) \equiv \pm\frac{d}{2} n_0' = \frac{1}{2(\pi D'')^{1/2}} \left[\int\limits_{\substack{-\infty \\ \text{interior}}}^{\theta'} \frac{d\theta' S_{\rm int}(\theta)}{(\theta^* - \theta)^{1/2}} - \int\limits_{\substack{-\infty \\ \text{exterior}}}^{\theta^*} \frac{d\theta' S_{\rm ext}(\theta)}{(\theta^* - \theta)^{1/2}} \right], \qquad \text{(A-5)}$$

where the $+(-)$ sign is for regions I and IV (II and III). Now we observe that at a given point on the separatrix $S_{\rm int} = -S_{\rm ext}$, which is required if the sum of Eqs. (A-1) and (A-2) is to satisfy Eq. (10) and yield a solution over all space (note in Eq. (A-1) $n = 0$ in exterior

region, and in Eq. (A-2) $n = 0$ in interior region). Thus, along a streamline with $\theta' = 0$ at the beginning of the quadrant that θ^* is in

$$\begin{aligned} S_{\text{int}}(\theta') &= -S_{\text{ext}}(\theta'), & &\begin{cases} 0 < \theta' \bmod (1) < \theta^*, \\ 1/4 < -\theta' \bmod (1) < 1/2 \end{cases} \\ S_{\text{int}}(\theta') &= -S_{\text{ext}}\left(\theta' + \frac{1}{2}\right), & &\begin{cases} 0 < -\theta' \bmod (1) < 1/4, \\ 1/2 < -\theta' \bmod (1) < 3/4. \end{cases} \end{aligned} \tag{A-6}$$

We also observe that $S_{\text{int}}(\theta^*) = -S_{\text{int}}(\theta^* + 1/2)$ as the global inversion symmetry of Eq. (7) for this flow pattern allows an antisymmetric solution for n, which requires an equal strength source and sink at θ^* and $\theta^* + 1/2$, respectively. Now we break up the integrals into sums along various sectors. We define

$$\begin{aligned} 2(\pi D'')^{1/2} K_1(\theta^*, \theta) &= \frac{H(\theta^* - \theta')}{(\theta^* - \theta')^{1/2}} + \sum_{m=1}^{\infty} \frac{1}{(\theta^* - \theta' + m)^{1/2}} \\ 2(\pi D'')^{1/2} K_2(\theta^*, \theta) &= \sum_{m=0}^{\infty} \frac{1}{(\theta^* - \theta' + m + 1/4)^{1/2}} \\ 2(\pi D'')^{1/2} K_3(\theta^*, \theta) &= \sum_{m=0}^{\infty} \frac{1}{(\theta^* - \theta' + m + 1/2)^{1/2}} \\ 2(\pi D'')^{1/2} K_4(\theta^*, \theta) &= \sum_{m=0}^{\infty} \frac{1}{(\theta^* - \theta + m + 3/4)^{1/2}} \end{aligned} \tag{A-7}$$

with

$$H(x) = \begin{cases} 1, & x > 0 \\ 0, & x < 0. \end{cases}$$

Equation (A-5) for the four sectors becomes

$$\begin{aligned} (\pi D'')^{1/2} \frac{n_0' d}{2} &= 2\hat{K}_1 \mathrm{S(I)} + \left(\hat{K}_2 + \hat{K}_4\right) \mathrm{S(IV)} + 2\hat{K}_3 \mathrm{S(III)} + \left(\hat{K}_2 + \hat{K}_4\right) \mathrm{S(II)} \\ -(\pi D'')^{1/2} \frac{n_0' d}{2} &= 2\hat{K}_1 \mathrm{S(II)} + \left(\hat{K}_2 + \hat{K}_4\right) \mathrm{S(I)} + 2\hat{K}_3 \mathrm{S(IV)} + \left(\hat{K}_2 + \hat{K}_4\right) \mathrm{S(III)} \\ -(\pi D'')^{1/2} \frac{n_0' d}{2} &= 2\hat{K}_1 \mathrm{S(III)} + \left(\hat{K}_2 + \hat{K}_4\right) \mathrm{S(II)} + 2\hat{K}_3 \mathrm{S(I)} + \left(\hat{K}_2 + \hat{K}_4\right) \mathrm{S(IV)} \\ (\pi D'')^{1/2} \frac{n_0 d}{2} &= 2\hat{K}_1 \mathrm{S(IV)} + \left(\hat{K}_2 + \hat{K}_4\right) \mathrm{S(III)} + 2\hat{K}_3 \mathrm{S(II)} + \left(\hat{K}_2 + \hat{K}_4\right) \mathrm{S(I)}, \end{aligned} \tag{A-8}$$

where

$$\hat{K}_j \mathrm{S(i)} = \int_0^{1/4} d\theta' K_j(\theta^*, \theta') S(\theta')_{\text{sector i}}$$

and $S(\theta')_{\text{sector i}} = S_{\text{int}}(\theta')$ in the ith quadrant, with $\theta' = 0$ at the beginning of the sector that θ^* is in. Now, as S(I) = −S(III) and S(II) = −S(IV), we then have for S(II) (or S(III))

$$\begin{aligned} -(\pi D'')^{1/2} \frac{n_0' d}{2} &= \left(\hat{K}_1 - \hat{K}_3\right) \mathrm{S(II)} \\ &= \int_0^{\theta} \frac{d\theta' S_{\text{int}}(\theta')}{(\theta - \theta')^{1/2}} + \sum_{m=1}^{\infty} (-1)^m \int_0^{1/4} \frac{S_{\text{int}}(\theta) d\theta'}{[m/2 + (\theta - \theta')]^{1/2}}. \end{aligned} \tag{A-9}$$

This is just Eq. (19) for $\beta = 1$ for which we have obtained a solution. Then using $\int u dl = \pi u d$, we may solve for the total flux along the separatrix and obtain

$$D^* = \left(\frac{\mathrm{Dud}}{2}\right)^{1/2} \frac{1}{A(.5)} = .944(\mathrm{Dud})^{1/2}. \tag{A-10}$$

This result has also been obtained in Ref. 15. Note that our original method of solution has been generalized to this more complex problem even though n varies along the separatrix.

References

1. S. Chandrasekhar, **Hydrodynamic and Magnetohydrodynamic Stability**, Dover Publications, Inc. (New York, 1961).
2. M. J. Lighthill, Proc. R. Soc. **A202**, 359 (1950).
3. G. I. Taylor, Proc. R. Soc. **A219** (1953).
4. G. W. Morgan, A. C. Pipkin, and W. H. Werner, J. Aero. Sci. **25**, 173 (1958).
5. R. Ariz, Proc. R. Soc. **A235**, 67 (1956).
6. A. Acrivos and J. D. Goddard, J. Fluid Mechanics **23**, 273 (1965).
7. W. Horton, Plasma Physics **23**, 1107 (1981).
8. W. Horton, "Drift Wave Turbulence and Anomalous Transport," in **Handbook of Plasma Physics II**, eds. M. N. Rosenbluth and R. Z. Sagdeev, North Holland (Amsterdam, 1984) 384–402.
9. H. K. Moffat, Rep. Prog. Phys. **46**, 621 (1983).
10. F. W. Perkins and E. G. Zweibel, Phys. Fluids **30**, 1079 (1987).
11. J. Gollob and T. Solomon, **Chaos Related Nonlinear Phenomena**, Procaccia ed., Plenum N. Y. (1987).
12. B. Walden, P. Kolodner, A. Passner, and C. Surko, Phys. Rev. Lett. **55**, 496 (1985).
13. H. Swinney and W. Y. Tam, to be published, Phys. Rev. A **36**, (July, 1987).
14. F. Sagues and W. Horsthemke, Phys. Rev. **A34**, 4136 (1986).
15. A. Nadim, R. G. Cox, and H. Brenner, J. Fluid Mech. **164**, 185 (1986).
16. B. Schraiman, to be published, Physical Review A, (1987).
17. T. H. Pollard, Numerical and Statistical Techniques, Cambridge, 1977.

Figure Captions

Fig. 1 Circulation pattern for rolls with a periodicity $2d$ in x-direction and $2d/\beta$ in y-direction.

Fig. 2 Schematic density profile for the dye along x-direction. Steep transistions in the density exist between each cell.

Fig. 3 The running diffusion coefficient for a typical initial value simulation for $D = 0.9$.

a) Particle distribution in the $x - y$ plane.

b) The running diffusion coefficient $D^*(t)$ as a function of time.

Fig. 4 The correlation function is plotted against time, measured in kicks in an initial value simulation. In this case, $\tau_H = 20\tau_K$.

Fig. 5 Measured effective diffusion coefficient D^* as a function of D in an initial value simulation. 200 particles using the χ^2 test and no regression fit. The range where the square root law applies ($D \leq .5$) is expanded on the left. If no error bar is shown then the error bar is too small to show on this scale.

Fig. 6 Typical plots for the steady-state method. Here, 250 particles are advanced $7000\tau_K$ with $x_0 = \pi$, $D = 0.02$.

a) Number of particles, N_e, escaping the region $x < |x_0|$ between times t and $t + 20\tau$ plotted against t measured in kicks.

b) Histogram of N_e for the case in Fig. 7a. F_{Ne} is the number of times that N_e particles escaped in $20\tau_K$. The dashed line shows the Gaussian fitted to the distribution.

Fig. 7 D^* plotted against D for the steady-state method. The range $D \leq .5$ is expanded on the left. If no error bar is shown then the error bar for that point is too small to show on this scale.

Fig. 8 Schematic diagram of the circulation pattern from rotating cylinders.

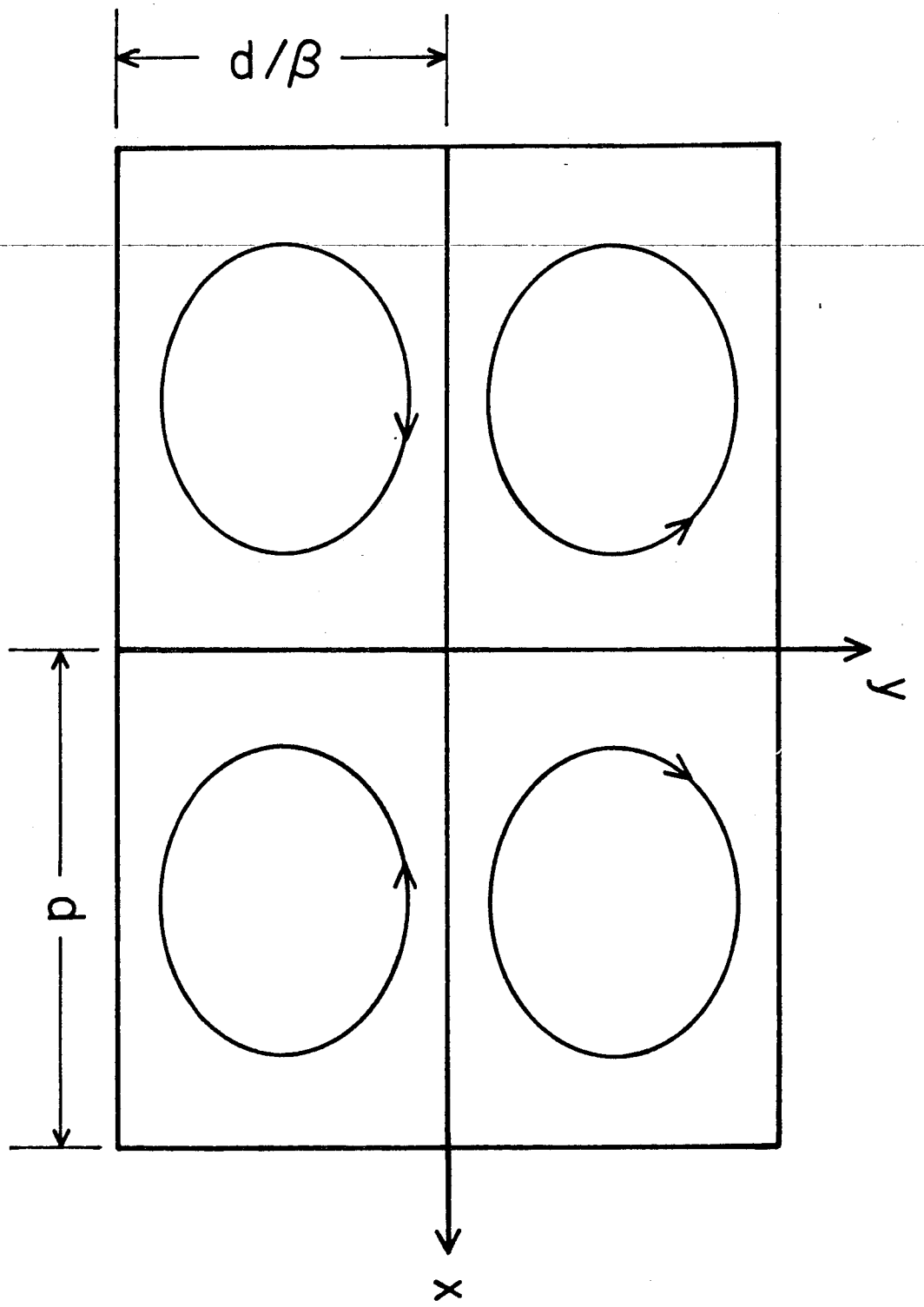

Fig. 1

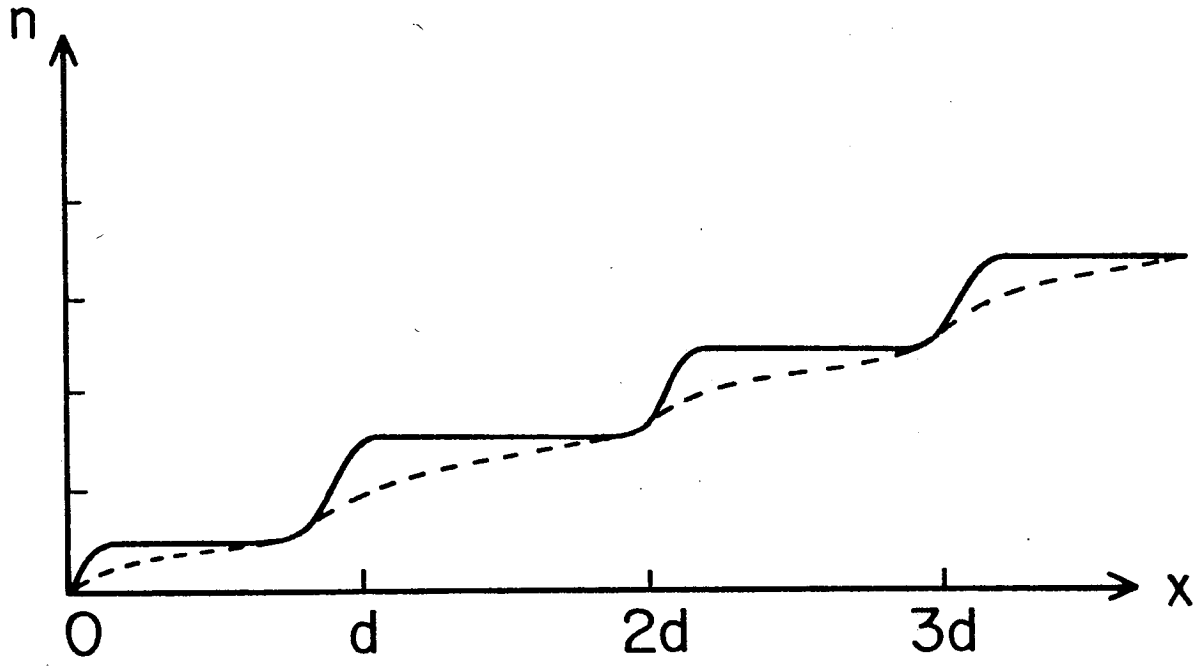

Fig. 2

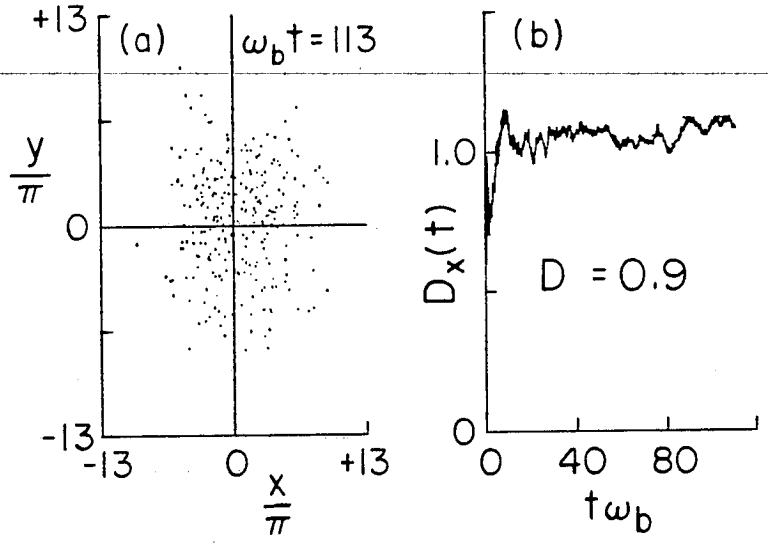
+13
(a)
$\omega_b t = 113$
$\frac{y}{\pi}$
0
-13
-13
0
+13
$\frac{x}{\pi}$
(b)
1.0
$D_x(t)$
D = 0.9
0
0
40
80
$t\omega_b$

Fig. 3

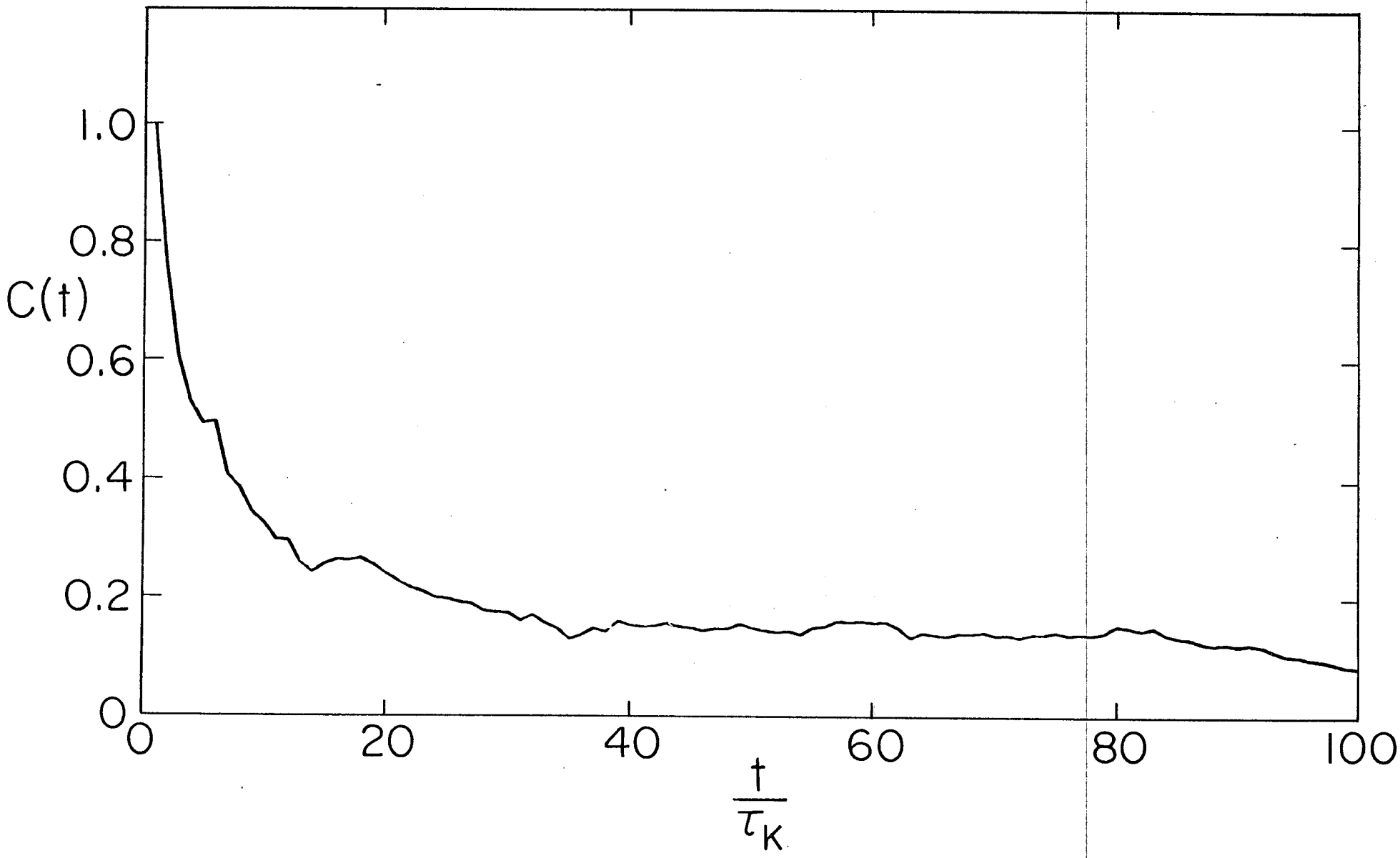

Fig. 4

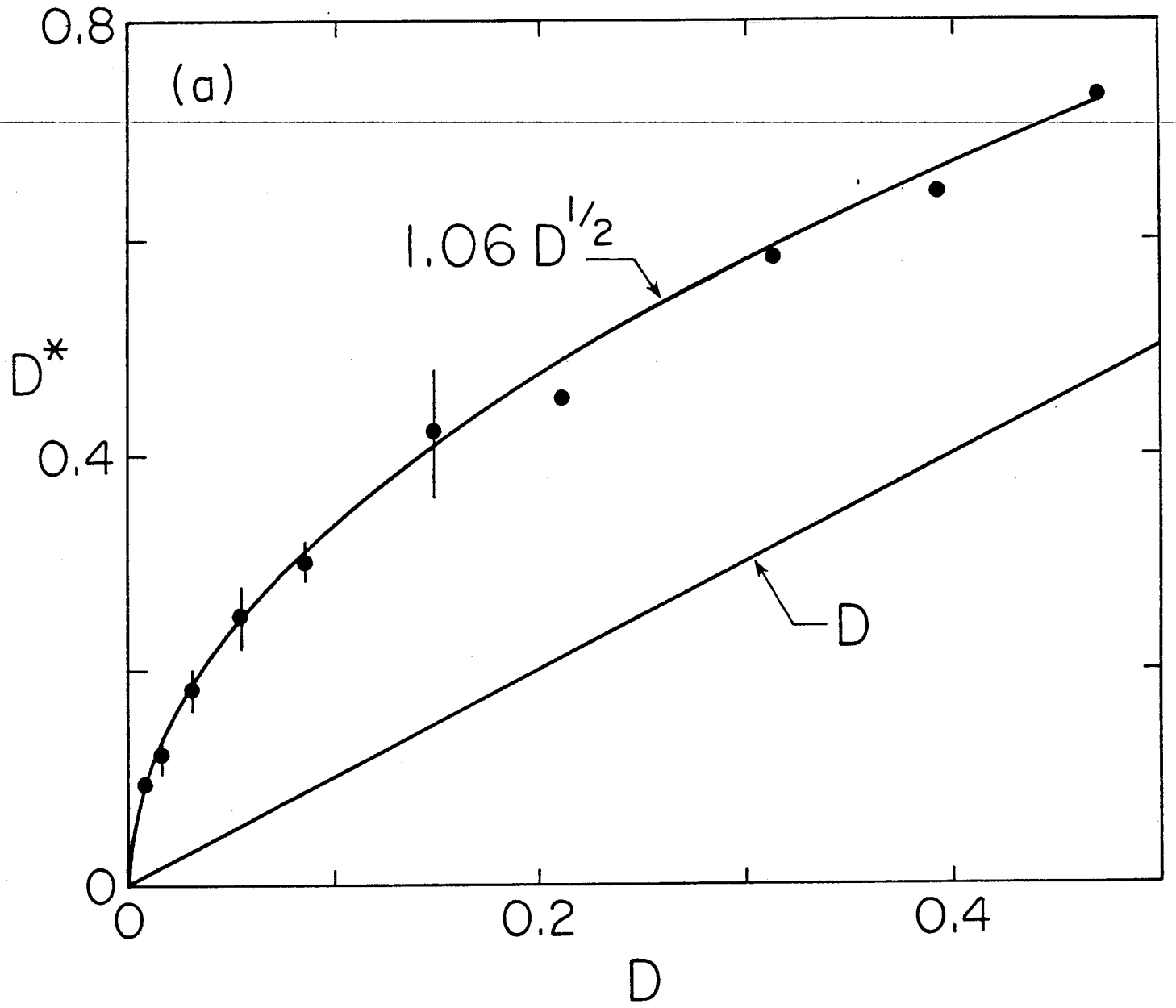

Fig. 5(a)

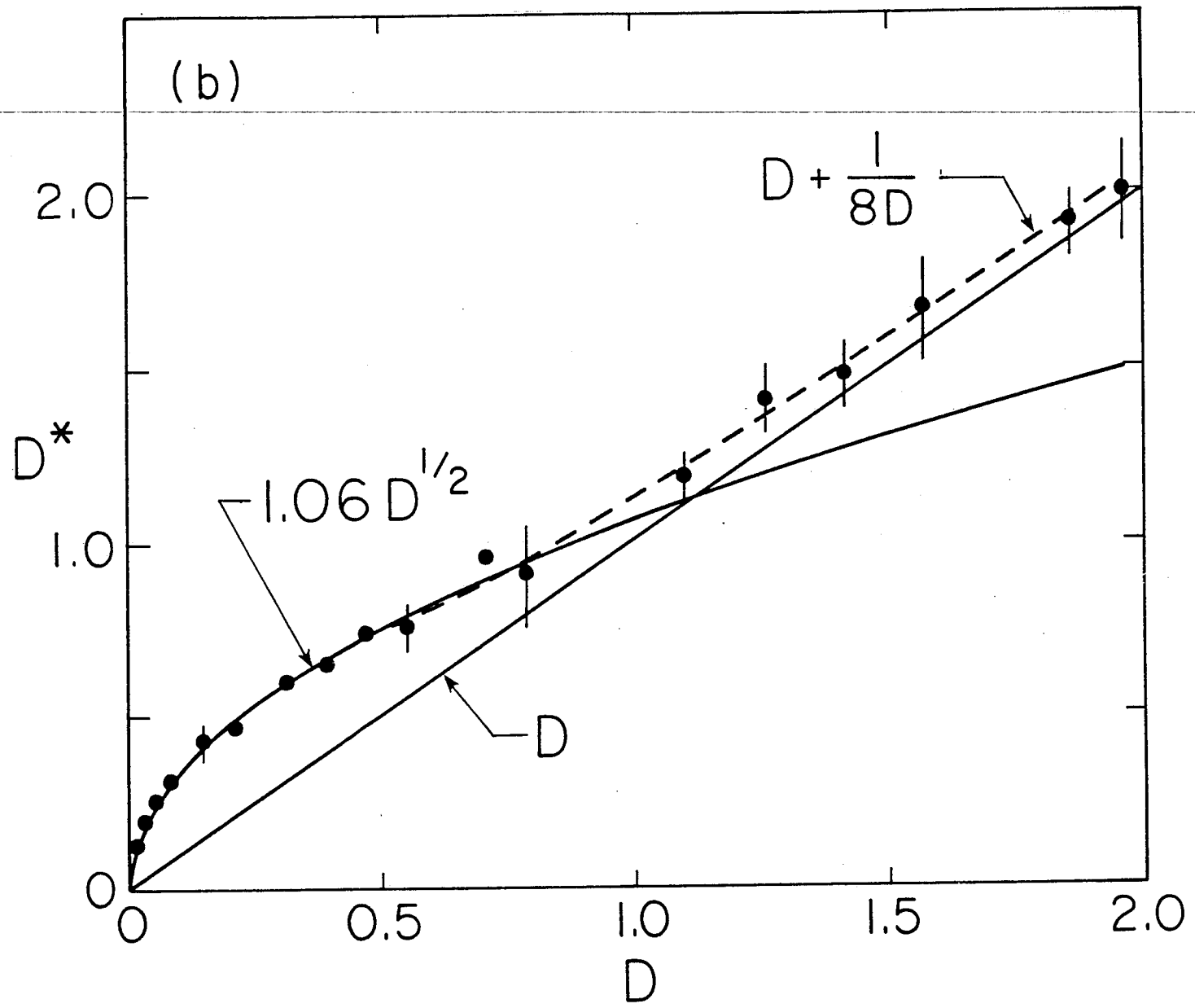

Fig. 5(b)

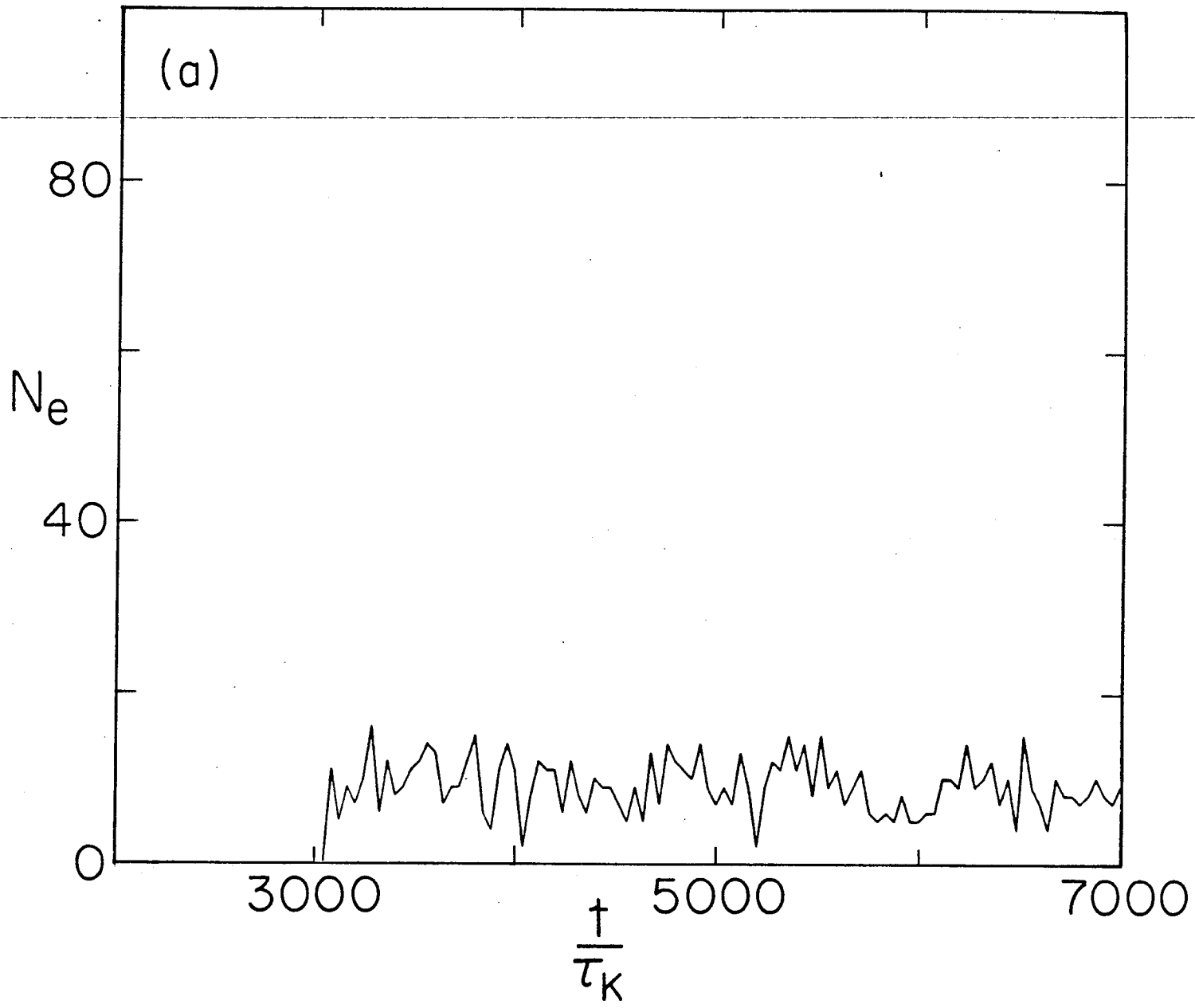

Fig. 6(a)

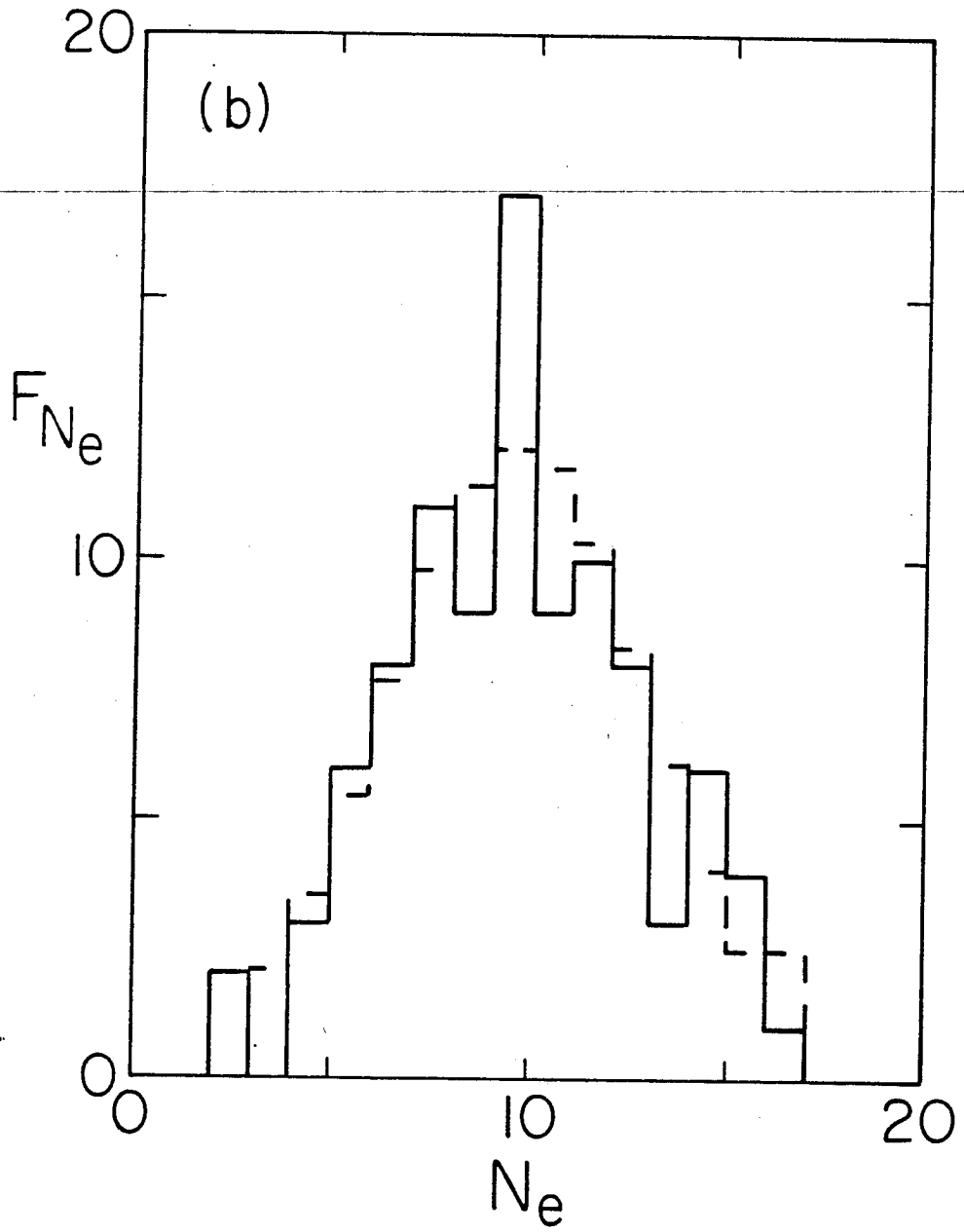

Fig. 6(b)

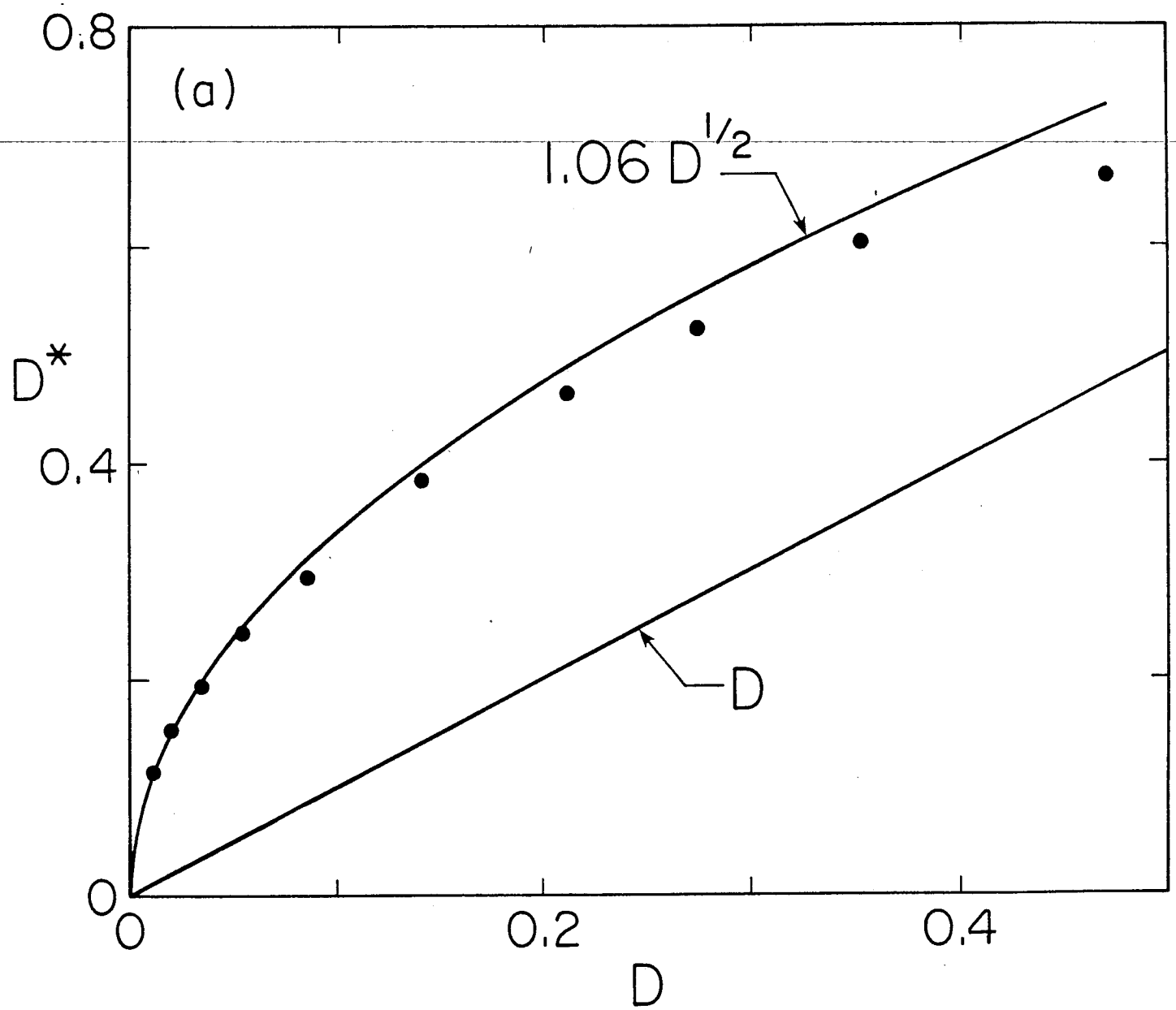

Fig. 7(a)

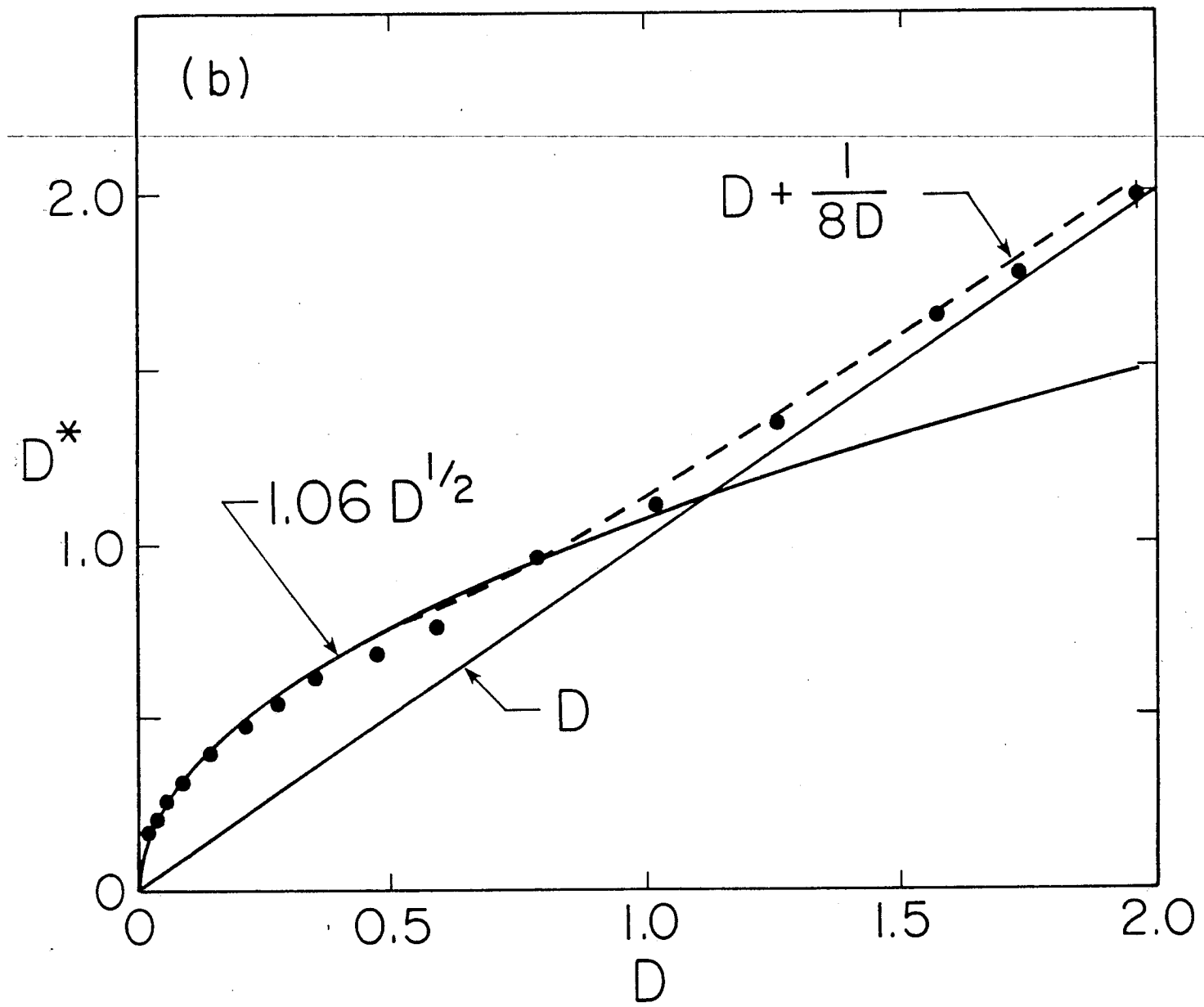

Fig. 7(b)

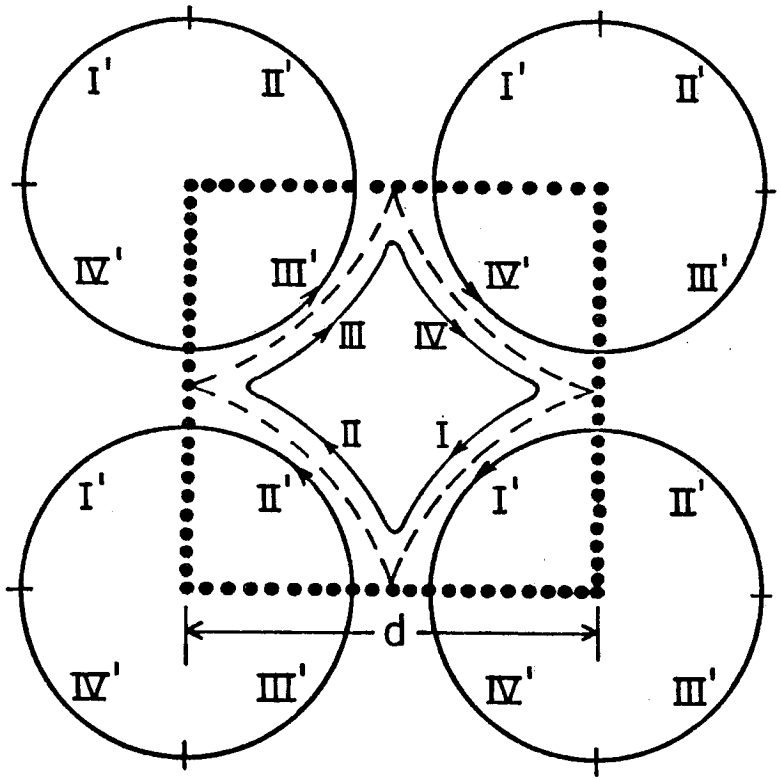

Fig. 8